Geochemistry, Geophysics, Geosystems

Supporting Information for

Mechanistic links between the sedimentary redox cycle and marine acid-base chemistry

Christopher T. Reinhard[1,2] and Woodward W. Fischer[3]

[1]School of Earth & Atmospheric Sciences, Georgia Institute of Technology, Atlanta, GA, USA
[2]NASA Astrobiology Institute, Mountain View, CA
[3]Division of Geological & Planetary Sciences, California Institute of Technology, Pasadena, CA, USA

Contents of this file

Introduction

This Supporting Information provides a description of the quantitative Earth system model discussed in the main text and a series of model perturbations and sensitivity tests (Figures S1-S3), along with all equations (Table S1), climate system parameters (Table S2), detailed flux equations (Table S3), default parameter values (Table S4), and steady state reservoir and flux values following model spinup (Table S5).

Model description

The ocean-atmosphere system is formulated as a single, well-mixed reservoir at gas exchange equilibrium (Main Text Figure 1). Time-dependent mass balance expressions track the reservoirs of total ocean-atmosphere carbon, ocean alkalinity, marine calcium and sulfate, atmospheric oxygen, and the crustal reservoirs of organic carbon, carbonate carbon, pyrite sulfur, and evaporite sulfur (Table S1). We link the Earth surface sulfur cycle and the acid-base balance of the ocean-atmosphere system via terms that express the relative partitioning of the H^+ equivalents generated through the oxidation of crustal sulfide minerals through either crustal carbonate dissolution, crustal silicate weathering, or an 'unbuffered' flux of H^+ equivalents directly to the oceans.

Because many of the important crustal weathering fluxes at Earth's surface depend on surface temperature and/or runoff [*Berner et al.*, 1983; *Kump and Garrels*, 1986; *Bergman et al.*, 2004; *West*, 2012; *Maher and Chamberlain*, 2014], the model includes a simple climate system that is governed by a base radiative temperature, described according to a single-layer grey atmosphere at radiative equilibrium [*Chamberlain*, 1980]. This is modified by additional radiative forcing that depends on atmospheric greenhouse gas content (e.g., pCO_2, pCH_4, and pN_2O). This atmospheric forcing is then scaled by a parameter specifying the equilibrium climate sensitivity to radiative forcing (Table S2). The atmospheric greenhouse effect employs recently derived radiative forcing fits for CO_2, CH_4, and N_2O [Table S2; *Byrne and Goldblatt*, 2014]. For all simulations presented here, we employ the reference pCO_2, pCH_4 and pN_2O values from [*Byrne and Goldblatt*, 2014], with solar luminosity at a value pertaining to 750 Mya.

The weathering of crustal silicate and carbonate minerals is parameterized following *Mills et al.* [2011], and specifies an overall weathering rate controlled by a kinetic weathering term and a maximum weathering rate meant to represent 'transport limited' weathering at very high rates of erosion [e.g., *West et al.*, 2005]. Weathering rates in the kinetically limited regime respond to both changes in temperature (implicitly accounting for kinetic effects and changes in runoff) and directly to atmospheric CO_2 levels, and are further modulated by terms describing the relative weatherable amounts of each phase at the Earth surface and, in the case of carbonates, by relative changes in the overall size of the crustal carbonate reservoir (Table S3).

Carbonate burial in the marine system is controlled by the average ocean saturation state with respect to calcite, a reference carbonate saturation state towards which the ocean carbonate system will relax through either carbonate burial or seafloor carbonate dissolution (e.g., 'carbonate compensation'), and a 'pseudo-reaction order' for carbonate precipitation (Table S3). It is important to note that this approach implicitly assumes that there is an effectively limitless reservoir of carbonate sediment available at the seafloor to buffer the ocean carbonate system, which in the case of very extreme and/or protracted perturbations may not be the case [*Archer et al.*, 1997].

The chemical alteration of seafloor basaltic rocks is parameterized as a function of bottom water chemistry through kinetic rate laws for mineral dissolution promoted by H^+, OH^-, and H_2O [Table S3; *Le Hir et al.*, 2008]. In this formulation, the overall dissolution rate of basaltic crust is summed over all dissolving species, each of which catalyzes dissolution as a function of a given activation energy, dissolution rate constant, species activity, and reaction order for each dissolution reaction. Values for activation energy, reaction order, rate constants, and mineralogy of the basaltic crust are identical to those implemented in *Le Hir et al.* [2008], while species activities are calculated at each timestep according to marine carbonate chemistry.

In general, the chemical weathering of petrogenic organic carbon and reduced sulfur in crustal sulfide minerals is thought to respond to levels of atmospheric O_2. However, the sensitivity of these processes to atmospheric pO_2 is not particularly well constrained and is subject to debate. We parameterize both petrogenic organic carbon and crustal sulfide weathering as saturation functions with respect to atmospheric O_2 levels, modulated by a weatherability parameter and the overall crustal reservoir size (Table S3). We specify a series of scaling constants chosen such that weathering fluxes relative to those of the modern Earth saturate at a prescribed pO_2 value and that some finite weathering flux persists to very low pO_2 values. This parameterization is meant to simultaneously contrast the weathering of reduced C and S in the crust while accounting for the fact that the oxidative weathering of both phases is often transport-limited on the modern Earth [*Petsch et al.*, 2000; *Wildman et al.*, 2004; *Petsch et al.*, 2005; *Bolton et al.*, 2006]. We also explore a more conventional 'power law' parameterization of organic C and pyrite S weathering, where both phases are assumed to weather as a square-root functions of atmospheric pO_2 [$J_i \propto (pO_2/pO_2^0)^{0.5}$]. Results of these simulations are shown in Figure S3.

Burial of reduced C and S in marine sediments is parameterized to respond in a simple fashion to Earth surface O_2 levels [*Canfield*, 1994; *Hartnett et al.*, 1998; *Hedges et al.*, 1999]. In the case of organic carbon burial, we specify a series of scaling parameters such that relative organic C burial rates are equivalent to the modern above ~60% of the present atmospheric O_2 level (PAL), increase sharply below ~20% PAL, and saturate at roughly 6 times the modern organic C burial rate below ~1% PAL. This parameterization is based broadly on results from a more complex box model of ocean biogeochemistry [*Ozaki and Tajika*, 2013]. Burial of pyrite S is assumed to scale with organic C burial (and thus Earth surface O_2 levels), but is also modulated by the availability of SO_4^{2-} in seawater (Table S3). For simplicity, we adopt a linear dependence on seawater [SO_4^{2-}] here, but note that this relationship is more likely to be a 'saturation' function of some form. The results are not qualitatively affected by this parameterization. Finally, weathering of evaporites at Earth's surface is expected to scale with the overall crustal mass of evaporite minerals, while evaporite burial is parameterized as a function of the relative ion activity product of $CaSO_4$ under the broad assumption that with more sulfate in seawater marginal marine basins may produce sulfate evaporites more often (Table S3).

Prior to perturbation experiments a series of initial reservoir sizes and fluxes is chosen to arrive at a desired steady state, and the model is spun up for 30 Myr with no external forcing so that all crust-ocean-atmosphere reservoirs come to dynamic equilibrium. Perturbations are then applied to this steady state spinup (Table S5). For the sake of illustration, initial steady states are meant to approximate conditions of the 'late Proterozoic' Earth system—a time when major perturbations to redox cycling [*Reinhard et al.*, 2013] and acid-base fluxes [*Hoffman et al.*, 1998] are thought to have occurred. These conditions are different from modern in that the pyrite sulfur cycle is heightened relative to that inferred for the modern Earth, both relative to surface evaporite cycling and with respect to O_2 equivalent fluxes in the oxygen cycle (Table S5), consistent with isotopic data for Proterozoic (and potentially much of Phanerozoic) time [*Canfield*, 2005; *Halevy et al.*, 2012]. Because of the nature of proton equivalent mass balance in the model (Table S1), initial spinup conditions vary depending on how the effects of crustal sulfide oxidation reverberate through the rest of the system. However, spinups are designed principally to be similar in terms of Earth surface temperature (T_{surf}), carbonate saturation state (Ω), and the relative burial flux of reduced carbon (f_{org}).

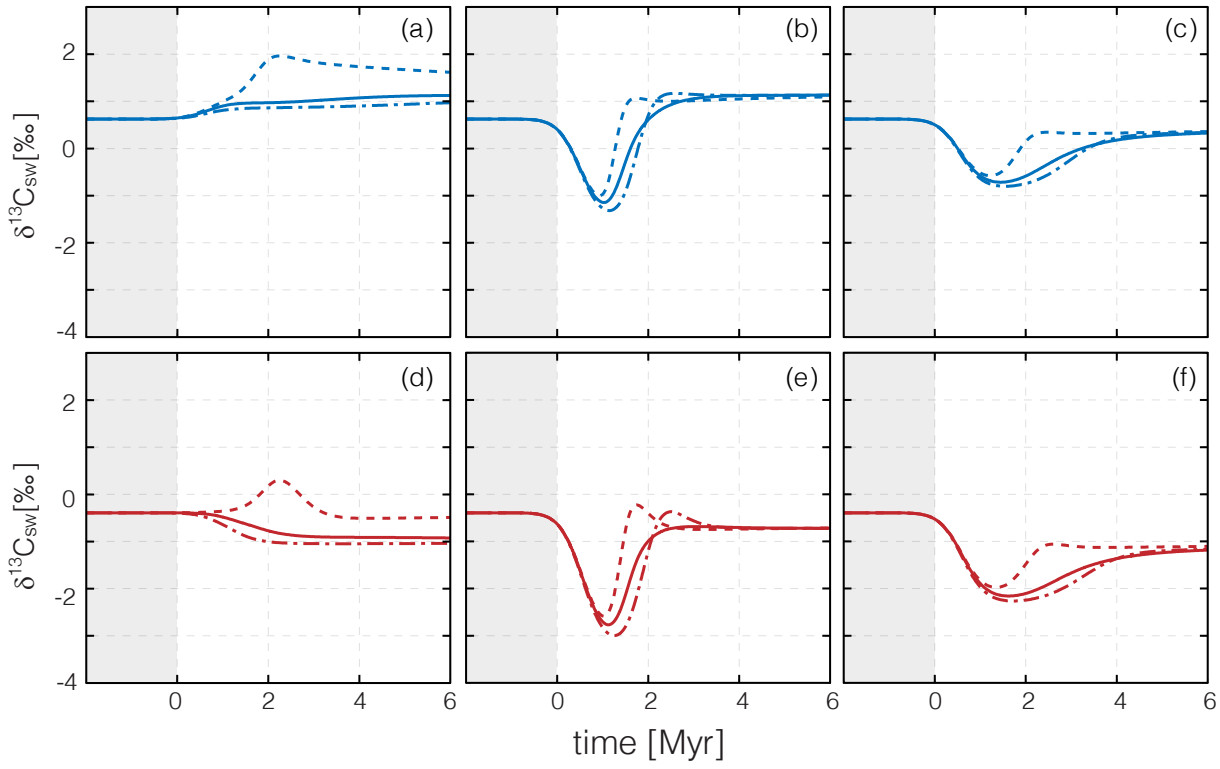

Figure S1. Time-dependent changes in the $\delta^{13}C$ of ocean-atmosphere total inorganic carbon for simulations identical to those shown in Main Text Figure 1. In all panels, a secular initial increase was applied to pyrite sulfur oxidation [doubling, (a),(d)], coupled pyrite sulfur and organic carbon oxidation [doubling, (b),(e)], and parallel weathering of all crustal phases represented in the model [50% increase, (c),(f)]. In (a)-(c), proton equivalents produced during crustal sulfide oxidation are channeled through carbonate dissolution, while in (d)-(f) they are channeled through crustal silicate dissolution. Dash-dot, solid, and dashed curves denote initial seawater SO_4^{2-} concentrations of 200 μM, 2 mM, and 20 mM, respectively.

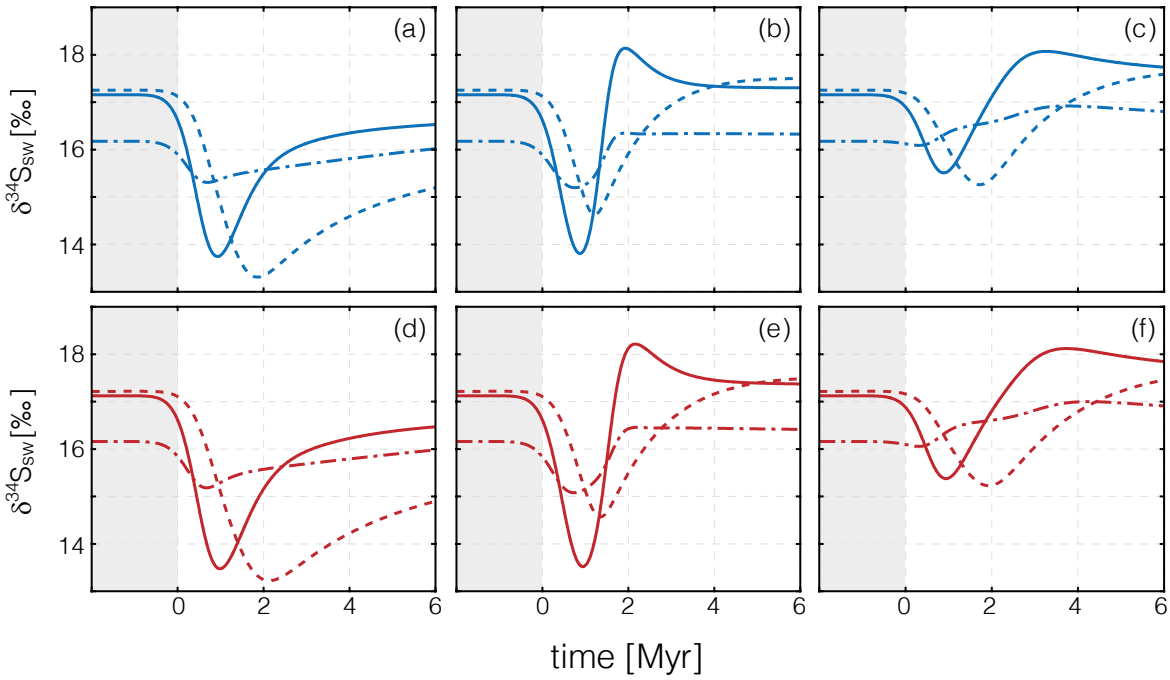

Figure S2. Time-dependent changes in the $\delta^{34}S$ value of seawater sulfate for simulations identical to those shown in Main Text Figure 1. In all panels, a secular initial increase was applied to pyrite sulfur oxidation [doubling, (a),(d)], coupled pyrite sulfur and organic carbon oxidation [doubling, (b),(e)], and parallel weathering of all crustal phases represented in the model [50% increase, (c),(f)]. In (a)-(c), proton equivalents produced during crustal sulfide oxidation are channeled through carbonate dissolution, while in (d)-(f) they are channeled through crustal silicate dissolution. Dash-dot, solid, and dashed curves denote initial seawater SO_4^{2-} concentrations of 200 μM, 2 mM, and 20 mM, respectively.

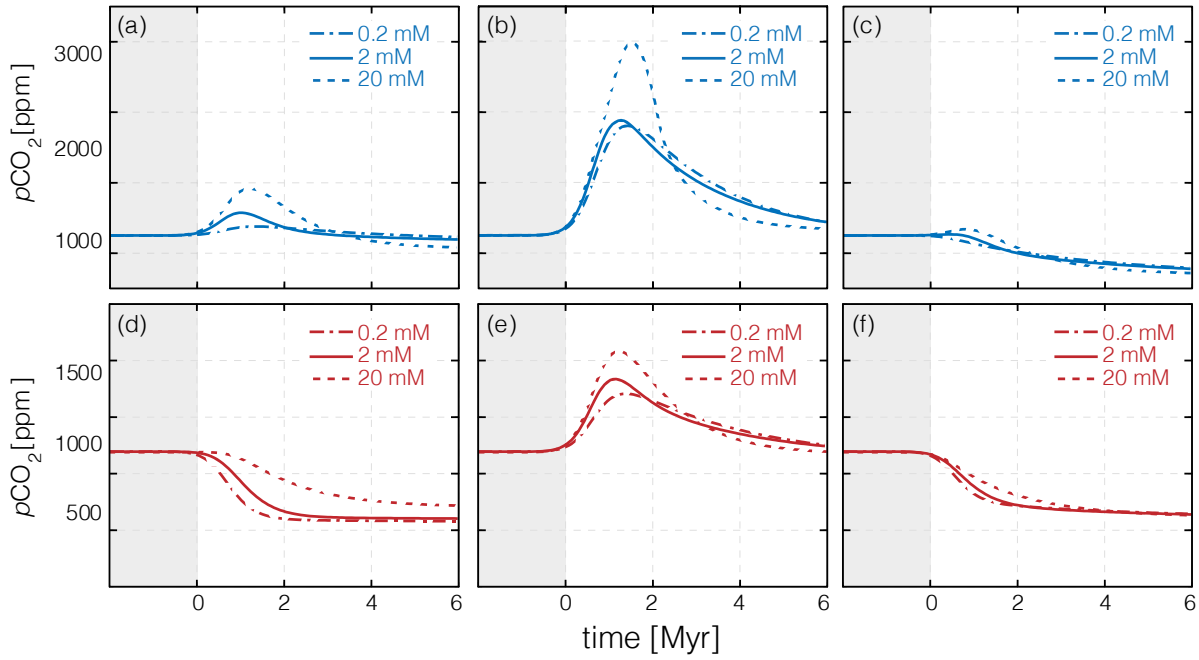

Figure S3. Simulations identical to those shown in Figure 1, but instead with a 'power-law' dependence of organic C and pyrite S weathering on atmospheric pO_2 (see text). In all panels, a secular initial increase was applied to pyrite sulfur oxidation [doubling, (a),(d)], coupled pyrite sulfur and organic carbon oxidation [doubling, (b),(e)], and parallel weathering of all crustal phases represented in the model [50% increase, (c),(f)]. In (a)-(c), proton equivalents produced during crustal sulfide oxidation are channeled through carbonate dissolution, while in (d)-(f) they are channeled through crustal silicate dissolution. Dash-dot, solid, and dashed curves denote initial seawater SO_4^{2-} concentrations of 200 µM, 2 mM, and 20 mM, respectively.

Table S1. Mass balance equations for model reservoirs. Masses in Tmol and fluxes in Tmol y^{-1}.

Description	Equation
ocean-atmosphere carbon	$\frac{dM_C^T}{dt} = \left[J_{volc} + J_{MOR} + J_{cc}^w + J_{org}^w + 2\gamma_{py}^{cc} J_{py}^w\right] - \left[J_{cc}^b + J_{org}^b + J_{crust}^b\right]$
oceanic alkalinity	$\frac{dM_{Alk}}{dt} = \left[2J_{sil}^w + 2J_{cc}^w + 2J_{py}^b + 2\gamma_{py}^{cc} J_{py}^w\right] - \left[2J_{cc}^b + 2\gamma_{py}^{H^+} J_{py}^w\right]$
oceanic calcium	$\frac{dM_{Ca^{2+}}}{dt} = \left[J_{sil}^w + J_{cc}^w + J_{py}^w\left(\gamma_{py}^{sil} + \gamma_{py}^{cc}\right) + J_{ev}^w\right] - \left[J_{cc}^b + J_{ev}^b\right]$
oceanic sulfate	$\frac{dM_{SO_4^{2-}}}{dt} = \left[J_{py}^w + J_{ev}^w\right] - \left[J_{py}^b + J_{ev}^b\right]$
atmospheric oxygen	$\frac{dM_{O_2}}{dt} = \left[J_{org}^b + r_{O:S} J_{py}^b\right] - \left[J_{org}^w + r_{O:S} J_{py}^w\right]$
petrogenic organic carbon	$\frac{dC_{ORG}}{dt} = J_{org}^b - J_{org}^w$
crustal carbonate carbon	$\frac{dC_{CC}}{dt} = J_{cc}^b - J_{cc}^w$
crustal pyrite sulfur	$\frac{dS_{PY}}{dt} = J_{py}^b - J_{py}^w$
crustal evaporite sulfur	$\frac{dS_{EV}}{dt} = J_{ev}^b - J_{ev}^w$
ocean-atmosphere carbon isotope composition	$\frac{d}{dt}\delta^{13}C_{sw} = \left[\sum_i \left(J_i\left[\delta_i^{13} - \delta_{sw}^{13}\right]\right) - \sum_o \left(J_o\left[\delta_o^{13} - \delta_{sw}^{13}\right]\right)\right]\left[M_C^T\right]^{-1}$
seawater sulfate isotope composition	$\frac{d}{dt}\delta^{34}S_{sw} = \left[\sum_i \left(J_i\left[\delta_i^{34} - \delta_{sw}^{34}\right]\right) - \sum_o \left(J_o\left[\delta_o^{34} - \delta_{sw}^{34}\right]\right)\right]\left[M_{SO_4^{2-}}\right]^{-1}$

Table S2. Parameter equations for climate model.

Parameter	Value	Units
Earth surface temperature	$T_{surf} = T_{base} + \Gamma R_f$	K
base temperature	$T_{base} = \left[\frac{S(1-\alpha)}{4\sigma(1-0.5\varepsilon)}\right]^{0.25}$	K
solar luminosity	$S(t) = S_0\left[1 - 0.38\frac{t}{t_0}\right]^{-1}$	W m^{-2}
CO_2 radiative forcing	$R_C = 5.32\ln[C_t / C_0] + 0.39\ln[C_t / C_0]^2$	W m^{-2}
CH_4 radiative forcing [0.1 – 2.5 ppmv]	$R_M = 1173\left[\sqrt{M_t} - \sqrt{M_0}\right] - 71636\left[\sqrt{M_t} - \sqrt{M_0}\right]^2$	W m^{-2}
CH_4 radiative forcing [2.5 – 100 ppmv]	$R_M = 0.824 + \frac{4}{5}\ln[M_t / M_1] + \frac{1}{5}\ln[M_t / M_1]^2$	W m^{-2}
N_2O radiative forcing [0.1 – 2.5 ppbv]	$R_N = 3899\left[\sqrt{N_t} - \sqrt{N_0}\right] - 38256\left[\sqrt{N_t} - \sqrt{N_0}\right]^2$	W m^{-2}
N_2O radiative forcing [2.5 – 100 ppbv]	$R_N = 4.182 + 3\ln[N_t / N_1] + 0.5469\ln[N_t / N_1]^2$	W m^{-2}

Table S3. Flux equations. Terms with subscript *'0'* represent pre-perturbation spinup values.

Flux term	Equation
crustal silicate/carbonate weathering (*i = sil, carb*)	$\frac{J_i^w}{J_{i,0}^w} = \left(R_i^T - R_i^K\right)\left[1+\exp\left[-\psi_K\left(R_i^K - R_i^T\right)\right]\right]^{-1} + R_i^K$
kinetically limited crustal silicate weathering	$R_{sil}^K = f_{sil}^A \exp\left[0.09\left(T_{surf} - T_0\right)\right]\left[1+0.025\left(T_{surf} - T_0\right)\right]\left(\frac{p\mathrm{CO}_2}{C_0}\right)^{\gamma_{sil}}$
kinetically limited crustal carbonate weathering	$R_{cc}^K = f_{carb}^A\left[1+0.087\left(T_{surf} - T_0\right)\right]\left(\frac{C_{CC}}{C_{CC}^0}\right)\left(\frac{p\mathrm{CO}_2}{C_0}\right)^{\gamma_{cc}}$
marine carbonate burial	$J_{cc}^b = k_{cc}\mathrm{sign}\left(\Omega - \Omega_{ref}\right)\left[\mathrm{abs}\left(\Omega - \Omega_{ref}\right)^{n_{cc}}\right]$
carbon fixation into altered oceanic crust	$R_{crust} = \sum_i k_i \exp\left[\frac{-E_i}{RT_p}\right] a_i^{n_i}$
weathering of crustal organic carbon	$\frac{J_w^{org}}{J_{w,0}^{org}} = f_{org}^A \sigma_1^{org}\left(\frac{p\mathrm{O}_2}{\sigma_2^{org} + p\mathrm{O}_2}\right)\left(\frac{C_{ORG}}{C_{ORG}^0}\right)$
weathering of crustal pyrite sulfur	$\frac{J_w^{py}}{J_{w,0}^{py}} = f_{py}^A \sigma_1^{py}\left(\frac{p\mathrm{O}_2}{\sigma_2^{py} + p\mathrm{O}_2}\right)\left(\frac{S_{PY}}{S_{PY}^0}\right)$
burial of organic carbon in marine sediments	$\frac{J_b^{org}}{J_{b,0}^{org}} = \phi_1^{org} + \phi_2^{org}\exp\left[-R_{\mathrm{O2}} / \phi_3^{org}\right]$
burial of pyrite sulfur in marine sediments	$\frac{J_b^{py}}{J_{b,0}^{py}} = J_b^{org}\left(\frac{J_{org}^b}{J_{org,0}^b}\right)\left(\frac{[\mathrm{SO}_4^{2-}]}{[\mathrm{SO}_4^{2-}]_0}\right)$
weathering of sulfate evaporite	$\frac{J_{ev}^w}{J_{ev,0}^w} = f_{ev}^A\left(\frac{S_{EV}}{S_{EV}^0}\right)$
burial of sulfate evaporite	$\frac{J_{ev}^b}{J_{ev,0}^b} = \left[\frac{[\mathrm{Ca}^{2+}][\mathrm{SO}_4^{2-}]}{\mathrm{IAP}_0}\right]$
isotope discrimination during primary production	$\Delta_{org} = \left[\frac{80}{0.034 * p\mathrm{CO}_2}\right] - 33‰$
globally integrated isotopic difference between seawater sulfate and sedimentary pyrite	$\Delta_{py} = \Delta_{\max}\left(\frac{\left[\mathrm{SO}_4^{2-}\right]}{K_m^{\Delta} + \left[\mathrm{SO}_4^{2-}\right]}\right)$

Table S4. Model parameter values.

Parameter	Description	Default	Units
S_0	modern solar luminosity	1368	W m^{-2}
α	planetary albedo	0.3	-
σ	Boltzmann constant	5.67 x 10^{-8}	W m^{-2} K^{-1}
ε	atmospheric emissivity	0.773	-
Γ	climate sensitivity parameter	0.5	-
t	age	750	Mya
f_{sil}^{A}	relative weatherable area of silicate rock	1.0	-
f_{carb}^{A}	relative weatherable area of carbonate rock	1.0	-
R_{sil}^{T}	transport-limited silicate rock weathering rate [relative]	2.5	-
R_{carb}^{T}	transport-limited carbonate rock weathering rate [relative]	1.0	-
ψ_K	silicate/carbonate weathering rate constant	100	-
γ_{sil}	CO_2 exponent for silicate rock weathering	0.25	-
γ_{cc}	CO_2 exponent for carbonate rock weathering	0.25	-
k_{cc}	rate constant for marine carbonate burial	[tuned]	y^{-1}
Ω_{ref}	reference ocean saturation state	1.0	-
n_{cc}	exponent for marine carbonate burial	1.7	-
f_{org}^{A}	relative weatherable area of petrogenic organic carbon	1.0	-
f_{carb}^{A}	relative weatherable area of carbonate carbon	1.0	-
f_{py}^{A}	relative weatherable area of crustal sulfide minerals	1.0	-
f_{ev}^{A}	relative weatherable area of evaporite minerals	1.0	-
σ_1^{org}	scaling parameter for crustal organic carbon oxidation	1.01	-
σ_2^{org}	scaling parameter for crustal organic carbon oxidation	1 x 10^{-3}	-
σ_1^{py}	scaling parameter for crustal sulfide oxidation	1.0005	-
σ_2^{py}	scaling parameter for crustal sulfide oxidation	1 x 10^{-4}	-
ϕ_1^{org}	scaling parameter for marine organic carbon burial	1.0	-
ϕ_2^{org}	scaling parameter for marine organic carbon burial	5.0	-
ϕ_3^{org}	scaling parameter for marine organic carbon burial	0.075	-
$r_{O:S}$	O_2/S ratio for pyrite weathering/burial	1.875	mol/mol
k_{py}	saturation constant for pyrite burial dependence on $[SO_4^{2-}]$	10	µmol kg^{-1}
Δ_{max}	maximum global sulfate-pyrite fractionation	50	‰
K_m^{Δ}	half-saturation constant for S isotope fractionation	10	µmol kg^{-1}
Δ_{crust}	C isotopic offset between seawater and ocean crust	1.0	‰
$\delta^{13}C_{volc}$	C isotope composition of volcanic carbon flux	-6.0	‰
$\delta^{13}C_{MOR}$	C isotope composition of mid-ocean ridge carbon flux	-6.0	‰
$\delta^{13}C_{org}$	C isotope composition of crustal organic carbon	-25.0	‰
$\delta^{13}C_{carb}$	C isotope composition of crustal carbonate carbon	+1.0	‰
$\delta^{34}S_{py}$	S isotope composition of crustal pyrite	-15.0	‰
$\delta^{34}S_{ev}$	S isotope composition of crustal sulfate evaporite	+15.0	‰

Table S5. Initial model spinup conditions. Values are shown for default spinup ($[SO_4^{2-}]$ = 2000 µmol kg^{-1}); there are very slight differences in initial steady state for variable $[SO_4^{2-}]$ conditions, on the order of ~1-2 ppmv for pCO_2 and ~5-10 µmol kg^{-1} for [DIC], [Alk], and $[Ca^{2+}]$.

		γ_{py}^{carb} = 1.0	γ_{py}^{sil} = 1.0	
Term	**Description**	**Value**	**Value**	**Units**
J_{volc}	volcanic carbon flux	9.0	15.0	TmolC y^{-1}
J_{MOR}	mid-ocean ridge carbon flux	1.6	1.6	TmolC y^{-1}
J_{sil}^{w}	silicate rock weathering flux	9.0	10.0	TmolC y^{-1}
J_{cc}^{w}	carbonate rock weathering flux	10.0	11.0	TmolC y^{-1}
$J_{sil,py}^{w}$	sulfide-catalyzed silicate weathering flux	0.0	10.0	TmolC y^{-1}
$J_{carb,py}^{w}$	sulfide-catalyzed carbonate weathering flux	12.0	0.0	TmolC y^{-1}
$J_{H+,py}^{w}$	proton equivalent flux from sulfide weathering	0.0	0.0	Teq y^{-1}
J_{cc}^{b}	marine carbonate burial flux	31.0	26.0	TmolC y^{-1}
J_{crust}^{b}	carbon burial flux during seafloor alteration	1.6	1.7	TmolC y^{-1}
J_{org}^{w}	organic carbon weathering flux	9.0	8.0	TmolC y^{-1}
J_{py}^{w}	crustal pyrite weathering flux	6.0	5.0	TmolS y^{-1}
J_{org}^{b}	marine organic carbon burial flux	9.0	8.0	TmolC y^{-1}
J_{py}^{b}	marine pyrite sulfur burial flux	6.0	5.0	TmolS y^{-1}
f_{org}	organic carbon burial fraction	0.22	0.22	-
[DIC]	ocean DIC concentration	4740	4340	µmol kg^{-1}
[Alk]	ocean alkalinity concentration	4920	4500	µmol kg^{-1}
$[Ca^{2+}]$	ocean calcium concentration	11.6	11.4	mmol kg^{-1}
pH	ocean pH	7.76	7.74	-
Ω	average ocean saturation state (calcite)	1.88	1.63	-
$[SO_4^{2-}]$	ocean sulfate concentration	2.0	2.0	µmol kg^{-1}
pO_2	atmospheric partial pressure of O_2	0.10	0.10	atm
pCO_2	atmospheric partial pressure of CO_2	991	946	ppmv
pCH_4	atmospheric partial pressure of CH_4	0.715	0.715	ppbv
pN_2O	atmospheric partial pressure of N_2O	0.29	0.29	ppbv
T_{surf}	global average surface temperature	13.9	13.9	ºC
C_{ORG}^{0}	initial crustal mass of organic carbon	1.0×10^{9}	1.0×10^{9}	Tmol
C_{CC}^{0}	initial crustal mass of carbonate carbon	1.5×10^{10}	1.3×10^{10}	Tmol
S_{PY}^{0}	initial crustal mass of pyrite sulfur	2.0×10^{8}	2.0×10^{8}	Tmol
S_{EV}^{0}	initial crustal mass of evaporite sulfur	1.1×10^{7}	1.1×10^{7}	Tmol
$\delta^{13}C_{sw}$	C isotope composition of ocean-atmosphere total inorganic carbon	0.62	-0.40	‰
$\delta^{34}S_{sw}$	S isotope composition of seawater sulfate	17.6	17.6	‰

References:

Archer, D., H. Kheshgi and E. Maier-Reimer (1997), Multiple timescales for neutralization of fossil fuel CO2, *Geophysical Research Letters*, *24*, 405-408.

Bergman, N. M., T. M. Lenton and A. J. Watson (2004), COPSE: A new model of biogeochemical cycling over Phanerozoic time, *American Journal of Science*, *304*, 397-437.

Berner, R. A., A. C. Lasaga and R. M. Garrels (1983), The carbonate-silicate geochemical cycle and its effect on atmospheric carbon dioxice over the past 100 million years, *American Journal of Science*, *283*, 641-683.

Bolton, E. W., R. A. Berner and S. T. Petsch (2006), The weathering of sedimentary organic matter as a control on atmospheric O2: II. Theoretical modeling, *American Journal of Science*, *306*, 575-615.

Byrne, B. and C. Goldblatt (2014), Radiative forcing at high concentrations of well-mixed greenhouse gases, *Geophysical Research Letters*, *41*, 152-160.

Canfield, D. E. (1994), Factors influencing organic carbon preservation in marine sediments, *Chemical Geology*, *114*, 315-329.

Canfield, D. E. (2005), The early history of atmospheric oxygen: Homage to Robert M. Garrels, *Ann. Rev. Earth Planet. Sci.*, *33*, 1-36.

Chamberlain, J. W. (1980), Changes in the planetary heat balance with chemical changes in air, *Planetary and Space Science*, *28*, 1011-1018.

Halevy, I., S. E. Peters and W. W. Fischer (2012), Sulfate burial constraints on the Phanerozoic sulfur cycle, *Science*, *337*, 331-334.

Hartnett, H. E., R. G. Keil, J. I. Hedges and A. H. Devol (1998), Influence of oxygen exposure time on organic carbon preservation in continental margin sediments, *Nature*, *391*, 572-575.

Hedges, J. I., F. S. Hu, A. H. Devol, H. E. Hartnett, E. Tsamakis and R. G. Keil (1999), Sedimentary organic matter preservation: A test for selective degradation under oxic conditions, *American Journal of Science*, *299*, 529-555.

Hoffman, P. F., A. J. Kaufman, G. P. Halverson and D. P. Schrag (1998), A Neoproterozoic Snowball Earth, *Science*, *281*, 1342-1346.

Kump, L. R. and R. M. Garrels (1986), Modeling atmospheric O_2 in the global sedimentary redox cycle, *Am. J. Sci.*, *286*, 337-360.

Le Hir, G., Y. Goddéris, Y. Donnadieu and G. Ramstein (2008), A geochemical modelling study of the evolution of the chemical composition of seawater linked to a "snowball" glaciation, *Biogeosciences*, *5*, 253-267.

Maher, K. and C. P. Chamberlain (2014), Hydrologic regulation of chemical weathering and the geologic carbon cycle, *Science*, *343*, 1502-1504.

Mills, B., A. J. Watson, C. Goldblatt, R. Boyle and T. M. Lenton (2011), Timing of Neoproterozoic glaciations linked to transport-limited global weathering, *Nature Geoscience*, *4*, 861-864.

Ozaki, K. and E. Tajika (2013), Biogeochemical effects of atmospheric oxygen concentration, phosphorus weathering, and sea-level stand on oceanic redox chemistry: Implications for greenhouse climates, *Earth and Planetary Science Letters*, *373*, 129-139.

Petsch, S. T., R. A. Berner and T. I. Eglinton (2000), A field study of the chemical weathering of ancient sedimentary organic matter, *Organic Geochemistry*, *31*, 475-487.

Petsch, S. T., K. J. Edwards and T. I. Eglinton (2005), Microbial transformations of organic matter in black shales and implications for global biogeochemical cycles, *Palaeogeography, Palaeoclimatology, Palaeoecology*, *219*, 157-170.

Reinhard, C. T., N. J. Planavsky, L. J. Robbins, C. A. Partin, B. C. Gill, S. V. Lalonde, A. Bekker, K. O. Konhauser and T. W. Lyons (2013), Proterozoic ocean redox and

biogeochemical stasis, *Proceedings of the National Academy of Sciences USA*, *110*, 5357-5362.
West, A. J. (2012), Thickness of the chemical weathering zone and implications for erosional and climatic drivers of weathering and for carbon-cycle feedbacks, *Geology*, *40*, 811-814.
West, A. J., A. Galy and M. Bickle (2005), Tectonic and climatic controls on silicate weathering, *Earth and Planetary Science Letters*, *235*, 211-228.
Wildman, R. A., R. A. Berner, S. T. Petsch, E. W. Bolton, J. O. Eckert, U. Mok and J. B. Evans (2004), The weathering of sedimentary organic matter as a control on atmospheric O2: I. Analysis of a black shale, *American Journal of Science*, *304*, 234-249.